Cowl Length Variation on Performance Characteristics of a Single Expansion Ramp Nozzle

V. I. Yazhini* and Balusamy Kathiravan†
Madras Institute of Technology, Chennai 600 044, India
and
T. M. Muruganandam‡ and Kandasamy Jayaraman§
Indian Institute of Technology, Chennai 600 036, India

https://doi.org/10.2514/1.B38217

Experiments have been carried out to investigate the effect of cowl length variation on performance characteristics of a single expansion ramp nozzle. The performance parameters were estimated for cowl lengths of 0, 25, 50, 75, and 100% with respect to the horizontal length of the ramp. Experiments were conducted for different nozzle pressure ratios ranging between 1.5 and 9. The wall static pressure distribution data were measured from the tests to estimate the various performance parameters, such as axial thrust, normal force, gross thrust, thrust vectoring angle, and coefficient of pitching moment. High-speed schlieren imaging was used to visualize the flow separation and shock patterns and to measure the jet width. The flow was separated from the ramp wall up to a nozzle pressure ratio of 3 for all cowl cases. The shorter cowl length delays the downstream movement of shock-induced boundary separation inside the nozzle as compared to the longer cowl. The cowl trailing-edge flow was more underexpanded than the ramp tip flow. As cowl length increases, the increased restriction results in higher axial thrust and also increases the normal force. The pitching moment and thrust vectoring were dominated by normal force. Overall, as the nozzle pressure ratio increases, the axial force and jet width increase, whereas the normal force and the pitching moment increase up to a certain level and then decrease. As the cowl length increases, the axial thrust, normal thrust, pitching moment, and thrust vector angle increase, while the jet width decreases.

Nomenclature

A_t	=	nozzle throat area, mm^2
C_m	=	coefficient of pitching moment
$dF_{X,i}$	=	axial force or axial thrust acting on "i" port, N
$dF_{Y,i}$	=	normal force or normal thrust acting on "i" port, N
F_g	=	gross thrust, N
F_i	=	ideal thrust, N
F_X	=	axial force or axial thrust, N
F_Y	=	normal force, normal thrust, or lift force, N
H_t	=	throat height, mm
h_n	=	height of the nozzle, mm
J_w	=	jet width, mm
m_a	=	mass flow rate of the nozzle, kg/s
P	=	wall static pressure at a particular port, Pa
P_a	=	ambient pressure, Pa
P_o	=	stagnation pressure or settling chamber pressure, Pa
R	=	gas constant, $kJ/(kg \cdot K)$
T_o	=	stagnation temperature, K
V_t	=	velocity at the throat section, m/s
W	=	width of the nozzle, mm
X_i	=	axial distance of port location from the nozzle entry section, mm
X_j	=	axial distance measured along the jet from the ramp tip, mm
Y_i	=	normal distance of port location from the centerline axis, mm
β_i	=	convergent or divergent angle of the nozzle, deg
γ	=	specific heat ratio
Δl_i	=	center distance measured across the pressure port, mm
ΔX_i	=	axial distance measured across the pressure port, mm
ΔY_i	=	normal distance measured across the pressure port, mm
θ	=	thrust vectoring angle, deg
ρ_t	=	density at the throat section, kg/m^3

I. Introduction

AIR-BREATHING propulsion, like scramjet engines, synergetic air-breathing rocket engines, ramjets, and turborockets, has great potential for applications in military and space [1]. These engines have better performance, relative to rocket engines, in terms of specific impulse and weight reduction, since they use atmospheric oxygen for oxidizer, and thus they can carry heavier payload [2]. Proper designs of the aforementioned engines are required to optimize the thrust of the engine over wide operating conditions. Nonaxisymmetric single expansion ramp nozzles (SERNs) provide several benefits compared to axisymmetric nozzles in aerospace propulsion systems. The SERN can produce higher thrust with lesser frictional drag, along with a substantial reduction in overall weight of the scramjet engine. Further, the SERN provides flexibility to adjust the nozzle exit Mach number to attain better performance. The SERN consists of a top and lower plate attached with side walls, in which the top plate (called a ramp) may be convergent–divergent or divergent. The lower movable part of the SERN is called a cowl or flap; in this work, it is considered a cowl. The SERN also provides a combination of internal and external expansion systems, which gives superior performance [3]. Optimizing the SERN will result in the best possible performance. This will require understanding of the SERN flowfield over a wide range of operating conditions. Otter et al. [4] explained the advantages of using a nonaxisymmetric nozzle over the axisymmetric nozzle during flight conditions. The major benefit of using a noncircular configuration reduces the nacelle drag. Ruscher et al. [5] also stated that the SERN was more suitable for effective thrust vectoring and thrust reversal application.

*Postgraduate Student, Department of Aerospace Engineering; yazhi.exam@gmail.com.
†Teaching Fellow, Department of Aerospace Engineering; kathiravanb84@gmail.com. (Corresponding Author).
‡Professor, Department of Aerospace Engineering; murgi@smail.iitm.ac.in.
§Currently Visiting Professor, Department of Mechanical Engineering, Middle East Technical University, Turkey; jayaraman78@metu.edu.tr.

There is a large number of studies in the literature on SERNs. Many of them focus on two main aspects: geometrical parameter variations and flow characteristics. Re and Berrier [6] estimated the effect of geometry on the internal performance of the SERN at different nozzle pressure ratios (NPRs, defined as the ratio of the settling chamber pressure to the ambient pressure [7]). Performance associated with different flight conditions, thrust vectoring, and thrust reversals were reported. The results show that the SERN performed better than the nonaxisymmetric convergent–divergent nozzle, considering performance over both design and off-design conditions. Deere and Asbury [8] reported the effect of translating the throat on performance of the SERN at off-design conditions. The translation of the throat in turn explains the concept of the variable expansion ratio, such as low, intermediate, and high expansion ratios with a concave ramp. The nozzle with a higher expansion ratio shows improvement in thrust vector angle as compared with low-expansion-ratio nozzles. However, the thrust will decrease. Capone et al. [9] carried out parametric studies on SERNs at Mach numbers between 0.6 and 1.2. The parametric changes were carried out in both convergent–divergent and convergent nozzles by varying upper ramp length, ramp chordal angle, lower flap length, and flap chordal angle, as well as the axial and vertical locations of the nozzle throat. The convergent nozzle showed nearly constant thrust over the entire range of nozzle pressure ratios 1–12, while the convergent–divergent nozzle showed varying trends depending on the geometric variation. Damira et al. [10] carried out a computational study on the parametric optimization of the SERN by varying the cowl length, ramp length, and shape of the ramp and concluded that the increment in cowl length had better thrust. However, the flow physics were not explained.

Marathe and Thiagarajan [11] numerically investigated the influence of change in geometrical parameters, viz., the ramp angle (18, 20, and 22 deg) and cowl length (no cowl, $0.5h_n$, and h_n, where h_n is height of the nozzle) on the performance of the SERN for a fixed nozzle pressure ratio. The results showed that an increase in ramp angle had only marginal effect on thrust but increased the nose-up moment on the vehicle. The axial thrust and normal force were initially increasing with increasing cowl length up to a certain length, and on further increasing the cowl length, the normal force decreased. Thiagarajan et al. [12] simulated numerical studies on the SERN with various ramp angles and cowl geometry for the freestream Mach number of 6.5. The presence of the sidewall establishes two-dimensional-like flow and aids in the improvement of axial thrust. They found that increasing the cowl length increased the axial thrust. These works show that changing the ramp angle did not give any significant performance change, while an increase in flap length resulted in an increase in the thrust developed by the SERN.

Kumar and Rathakrishnan [13] examined the effect of side fence on the performance of the SERN. The performance parameters were estimated from the centerline wall static pressure measurements. They concluded that the nozzle without side fence generates more pressure thrust than that with side fence. Schirmer and Capone [14] experimentally studied the parametric variation on pitch and yaw vectoring angles along with the effect of the location of the sidewall hinge. The results show that the sideways deflection of the jet decreases the thrust. Yazhini et al. [15] studied the effect of the presence of a sidewall on internal performance characteristics of the SERN. The results show that the axial thrust was improved marginally without sidewalls. This is in contrast to earlier observations. This is because the shock wave from the lateral direction helped producing positive pressure on the ramp, producing thrust. Ruffin et al. [16] numerically studied the effect of the base model with side extension in the SERN. Watanabe [17] effectively conducted experiments to investigate the effect of hypersonic external flow interaction with the exhaust plume of the scramjet nozzle. The results show that the external flow suppresses boundary-layer separation on the ramp surface. Using a long side fence restricts the spanwise expansion and improves the thrust as compared to the shorter side fence. Xu et al. [18] studied overexpanded flow conditions using Particle Image Velocimetry (PIV) and numerical simulation. They tried capturing the flowfield using PIV but did not present data on variations of geometry or NPRs. It is evident that, in the literature, there has been a focus on geometric parameter

variation and observing its effect on the thrust produced. However, there was not enough focus on the effect of the change in geometry on the flowfield and, thus, the performance of the nozzle. The other performance parameters of practical interest, like the normal force, pitching moment, and thrust vectoring, were not studied in detail.

There were studies that focused on explaining the flowfield in the nozzle. Gruhn et al. [19] reported the performance of the SERN with aerodynamic flap design. They conducted wind-tunnel experiments with focus on the nozzle flowfield and boundary-layer separation for different NPRs and different Reynolds numbers, for flap with deflection. They did not show shock patterns for a wide range of NPRs. The results showed that the axial thrust coefficient decreases as the Mach number of the nozzle increases. At the same time, the thrust vectoring angle decreased by up to 15 deg for low Mach number conditions. Hiraiwa et al. [20] experimentally investigated the effect of ambient pressure on the thrust force and flow separation phenomena in the SERN. The thrust was estimated by using a load cell and the shear stress from stress-sensitive paint. The location of the boundary-layer flow separation and the pressure distribution were visualized. It was observed that the sidewall fence compresses the inlet flow and produces the crossing shock wave, causing flow separation at the ramp center. This flow separation moves upstream as the NPR increases, which increases the positive axial thrust force in the SERN.

Yu et al. [21] numerically studied the flow separation phenomena inside the SERN. The shock patterns were completely different from the axisymmetric nozzle's flow patterns. They also observed the appearance of restricted shock separation and free shock separation in a small range of NPRs. The shock separation affects the performance of the SERN, especially the lift force. Yu et al. [22] numerically simulated the flow separation phenomena of the SERN for the range of NPRs with separation in the ramp. The experimental flow separation pattern on the subscale SERN was compared with numerical simulations. The jet angle was found to vary based on the flow separation pattern. Lv et al. [23] numerically investigated the effect of fluidic secondary injection on the performance of the SERN. A secondary jet was injected from the cowl, which induces an incidence shock wave on the expansion ramp, improving the thrust, lift, and pitching moment of the SERN in off-design conditions.

Hirschen et al. [24–27] conducted experiments using the SERN to estimate the nozzle flow properties and thrust by pressure-sensitive paint and wall centerline pressure tappings. The effects of heat capacity ratio and wall temperatures were also studied in different studies. The pressure distribution measured from pressure-sensitive paint agreed well with the centerline wall pressure distribution, irrespective of Reynolds number and nozzle pressure ratio. The thrust from two-dimensional calculations was found to match the three-dimensional calculations using pressure-sensitive paint data within 2%, suggesting that there is not much change in performance due to three-dimensionality. Papamoschou et al. [28] and Tsunoda et al. [29] have also shown that using centerline wall static pressure data was sufficient even if the flow was to some extent three-dimensional. Hence, the centerline wall static pressure measurements are sufficient to predict the flow separation phenomena and shock motions inside the nozzle.

Zhang et al. [30] numerically studied the effect of nonuniform flow entry Mach number coupled with the shock wave and expansion wave on the thrust and lift generated by the SERN. Mo et al. [31] studied, both experimentally and computationally, the effect of nonuniform flow entry on performance characteristic of the SERN. The result indicates that the nonuniform flow entry nozzle improves the performance of the SERN, with marginal improvement in axial thrust but with significant improvement in lift and pitch moment. Hindash and Spaid [32] made an attempt to validate the computational performance of various turbulence models with experimental studies in the transonic regimes. The thrust coefficient predictions from various turbulence models were within 5% of the measurements from wind-tunnel tests.

From the preceding descriptions, it can be seen that there is no coherent effort on understanding the SERN flowfield for various
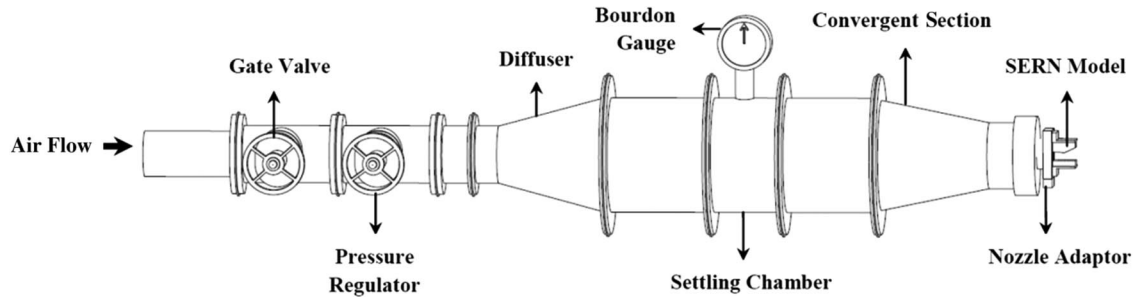
Fig. 1 Schematic representation of open jet facility.

pressure ratios and geometries and its effect on the performance parameters of the SERN. While there are a few works that attempt to do this, they worked on a narrow range of NPRs. There is no work that used both flow visualization and pressure measurements simultaneously to understand the flow behavior in a comprehensive manner. The present study is an attempt to understand the flowfield and assess the performance of the SERN designed for a low Mach number. Since the parametric variation can be exorbitant, this study focuses only on the cowl length variation. The effect of varying the cowl length on wall-pressure-based performance parameters, such as axial, normal, and gross thrust along the thrust vectoring direction, for different nozzle pressure ratios was studied. Schlieren flow visualization images were used to understand the flow behavior as well as different shock patterns.

II.   Experimental Details

A.   Open Jet Facility

The experiments were carried out using an open jet blowdown facility. Atmospheric air is compressed by a screw compressor, which can compress up to 12 bar at a rate of 1.5 kg/s. The moisture in the air is separated using a refrigeration-type dryer in line with the compressor. The dried compressed air from a reservoir was discharged through a gate valve and pressure-regulating valve into the settling chamber. The settling chamber had a diffuser cone and two grids at sufficient separation to reduce upstream fluctuations. The pressure inside the settling chamber was measured using both a Bourdon gauge with a least count of 20 kPa and a pressure tapping on the settling chamber wall. The working SERN model was mounted at the end of the settling chamber using a nozzle adapter, as shown in Fig. 1. The flow exits into atmosphere.

B.   Detail of SERN Models

A single expansion ramp nozzle with a constant width of 30 mm from inlet to exit was designed for an exit Mach number of 2. The nozzle consists of a constant area duct followed by a concave ramp with a convergent angle of 10.3 and a divergent angle of 25 deg. The bottom wall is just a straight-line wall, and all the area changes are through the top block. The angle is very close to the required turning angle (26.4 deg) for perfect $M = 2$ flow from the sonic throat. Thus, the flow just after the throat on the ramp is expected to be close to $M = 2$. Different cowl length variations were considered, as shown in Fig. 2. Cowl length is defined as the length from the throat to the end of the ramp in the horizontal direction. Cowl lengths of 0, 25, 50, 75, and 100% of the full divergent section of the nozzle were achieved by changing the bottom block of the nozzle. The length of the divergent ramp section was 26.4 mm. The dimensions and geometric details of the SERN for various cowl lengths are listed in Table 1 and shown Fig. 2. The nozzle has a rectangular cross-sectional inlet of 20×30 mm, a throat of 18×30 mm, and an exit area of 30×30 mm (exit can be defined clearly only for the 100% cowl case). The nozzle expansion area ratio was 1.688 for 100% cowl length; hence, the designed pressure ratio was 7.82.

C.   Wall Pressure Measurement

A Scanivalve pressure scanner (DSA3217) with 16 ports was used to measure the wall static pressure distribution with an accuracy of $\pm 0.01\%$ of the full scale (1 MPa). Experiments were conducted at different nozzle pressure ratios ranging from 1.5 to 9. The wall pressure tappings were made along the centerline of the nozzle for both ramp and cowl with equally spaced intervals of $\Delta x = 5$ mm. The ramp consists of a total of eight ports; the first pressure tapping was placed just 1 mm before the convergent section. This port location is taken as $X/H_t = 0$. Two ports were placed in the convergent section and five in the divergent section of the expansion ramp. Cowl ports were also arranged at same X locations as the ramp ports. The details of the pressure port locations in expansion and various cowl lengths are listed in Table 2. The throat location corresponds to $X/H_t = 0.722$. The uncertainty in the wall static pressure measurements was about 1.71%.

D.   Schlieren Flow Visualization Method

Schlieren visualization was used to capture the shock structure to understand the flow characteristics such as shock cell patterns, free shock separation, and flow deflection and also to estimate the jet width. The Z-type schlieren arrangement was made of two parabolic
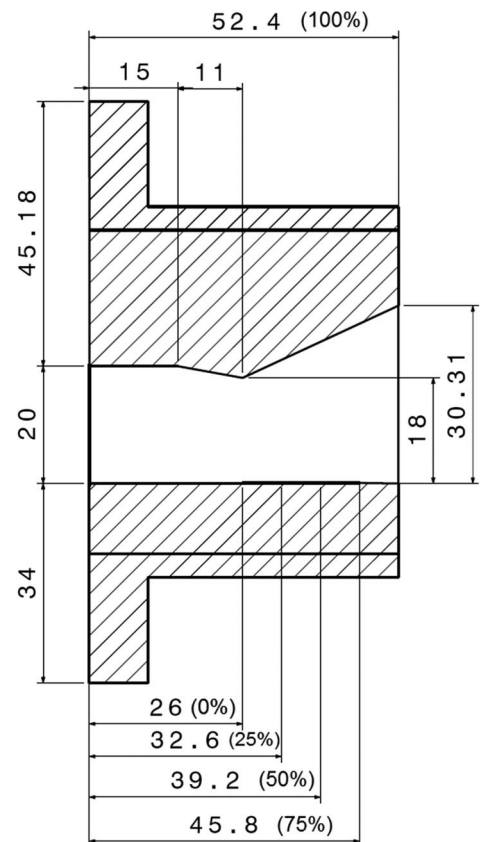

Fig. 2   Dimensions of nozzle section with various cowl length models. (All dimensions in mm.)

Table 1   Dimension of the single expansion ramp nozzle

S. No.	Descriptions	Measurements
01	Overall length of the nozzle	52.4 mm
02	Length of the constant area of the nozzle inlet	15 mm
03	Length of the convergent part of the ramp	11 mm
04	Length of the divergent part of the ramp	26.4 mm
05	Length of the 0% cowl from nozzle inlet	26 mm
06	Length of the 25% cowl from nozzle inlet	32.6 mm
07	Length of the 50% cowl from nozzle inlet	39.2 mm
08	Length of the 75% cowl from nozzle inlet	45.8 mm
09	Cross section of the nozzle inlet	20×30 mm
10	Cross section of the nozzle throat	18×30 mm
11	Cross section of the nozzle exit for 100% cowl length	30.31×30 mm
12	Convergent angle of the ramp	10.3 deg
13	Divergent angle of the ramp	25 deg

mirrors, a light source, and a knife edge. A high-speed camera (IDT MotionXtra N4) was used to capture the shock structure with a framing rate of 900 Hz and with an exposure time of 19 μs. The height of the throat was considered as the reference length for estimating the jet width of the nozzle using image-processing techniques.

III.   Results and Discussion

Experiments were conducted for all the five cowl length cases, for nozzle pressure ratios ranging from 1.5 to 9 in steps of 0.5. From inviscid one-dimensional calculations, the first critical pressure ratio (the NPR corresponding to the first time of nozzle choking) for this area ratio is 1.1, and the inviscid third critical pressure ratio (the NPR for perfectly expanded flow) is 7.64. This pressure ratio range will cover shock in the divergent section cases to underexpanded cases. In this section, wall static pressures are presented first, followed by the results of performance parameters, viz., axial force, normal force, gross thrust, pitching moment coefficient, thrust vectoring angle, and jet width, which were estimated from the wall static pressure distribution.

A.   Flowfield Study

This subsection attempts to explain the flowfield through wall pressure measurements and schlieren images. Figure 3 represents the wall static pressure distributions of various single expansion ramp nozzles for different cowl lengths. For clarity in the figures, nozzle pressure ratios 5.5, 6.5, 7.5, and 8.5 are omitted. The wall static pressure P distributions along the centerline direction of the SERN were measured. The measured wall static pressures were nondimensionalized with the settling chamber pressure P_o and plotted against the length along cowl X normalized by throat height H_t. This was done for five different cowl lengths. Solid lines show the ramp pressures, and dashed lines show the cowl pressures. Also, the two dashed lines shown in the plots are representing the throat location and the sonic pressure ratio. The first pressure port location is taken as

Table 2   Details of pressure port locations in the expansion ramp and in various cowl models

Port no.	Expansion ramp	0% cowl	25% cowl	50% cowl	75% cowl	100% cowl
			In terms of X/H_t			
01	0	0	0	0	0	0
02	0.278	0.278	0.278	0.278	0.278	0.278
03	0.556	0.556	0.556	0.556	0.556	0.556
04	0.833	——	0.833	0.833	0.833	0.833
05	1.111	——	——	1.111	1.111	1.111
06	1.389	——	——	1.389	1.389	1.389
07	1.667	——	——	——	1.667	1.667
08	1.9444	——	——	——	——	1.9444

$X/H_t = 0$. The throat location is at $X/H_t = 0.722$, as marked by a thin vertical line in the plots. The sonic pressure ratio is at $P/P_0 = 0.528$.

It was noticed from Fig. 3 that for most of the cases, flow enters the nozzle with the pressure ratios varied between 0.72 (corresponds to $M = 0.70$, from isentropic calculations) to 0.6 ($M = 0.88$), suggesting that the entry Mach number section of the SERN was high subsonic. This is close to the Mach number based on the area ratio in the subsonic side. This also shows that the incoming flow is not uniform from top to bottom, as shown by the wall pressures not being the same for ramp and cowl; higher velocities are seen in the cowl side. This type of flow was also observed by Schindel [33]. This may be due to the asymmetry in the nozzle profile. In the convergent section, the flow acceleration is higher on the cowl side as compared to its counterpart (the ramp). This may be related to the wall length being shorter and thus the effect of backpressure being felt better by the upstream flow. This argument is further supported by the fact that the 0% cowl case has the lowest pressure in the third pressure port. This case also has the highest deviation from the pressure on the ramp side as well, among all the cowl lengths. This suggests that the flow achieves sonic conditions just ahead of the $X/H_t = 0.68$ location in the 0% cowl length cases.

Even on the divergent side, the cowl pressures are not same as the ramp-side pressure for the same values of X/H_t. Typically, the pressure at the exit is same as the ambient pressure for most cases, both in the ramp and the cowl sides (exceptions occur at high nozzle pressure ratios). It can be seen that the pressures are continuously decreasing toward ambient in the cowl side, while in the ramp side, the pressures decrease slightly below ambient and then gradually increase until they reach the atmospheric pressure. This observation is also a result of the symmetry in the nozzle. The ramp side has expansion causes supersonic speeds followed by shock, which results in separated flows, while the cowl side experiences only a continuous expansion until the ambient pressure is achieved. Further, from the ramp-side pressures for different nozzle pressure ratios, it can be seen that the 0% cowl cases have the shock in diverging portion moving out, which is different from that of 100% cases. This can be explained only in conjunction with schlieren images as the flowfield determines this behavior, and schlieren data will be presented in the following paragraphs.

Figure 4 shows the horizontal knife-edge schlieren images of the flowfield for select cases. Images were obtained only for NPR 1.5, and for NPRs 2 to 9 in steps of 1. The ends of the side glass windows are also visible in the images, as the schlieren beam was having a slight inclination (~4 deg) to the plane of edges. Discussions will be presented for each nozzle pressure ratio, using both schlieren images and pressure data presented in Fig. 3, in the following paragraphs. The nozzle throat lies between ports 3 and 4 ($X/H_t = 0.722$). For nozzle pressure ratio 1.5 cases, the ramp pressure data for all the cases are almost identical. Even the cowl pressure data show similar trends as the 100% case for all nozzle pressure ratio 1.5 cases. The schlieren images for NPR 1.5 show that, after the throat section, the flow get separated; hence, the wall static pressure variations along the ramp became plateaued. The flow experiences a large turning angle of the wall at the throat on the ramp side, and the NPR is not enough to support it; thus, the flow separates, and the ramp wall experiences almost atmospheric pressure in the diverging portion. It can also be noted from the schlieren images that the separated shear layer from the throat is having an identical slope for both the images of Figs. 4a and 4b.

As the NPR was increased to 2, the flow gets choked in between ports 3 and 4, which was as expected. As the cowl length increases from 0 to 100%, the flow experiences very weak normal shock trains for all cowl lengths, as was already observed in literature [21,22]. The flow was still separated, as shown by the pressure data. As the NPR further increases from 2, the wall static pressure trends are similar on both the ramp and cowl, suggesting separated flow in the ramp, until the flow reaches NPR 3. This suggests that the expansion fans from the throat of the nozzle have increased the Mach number to supersonic flow near the cowl wall and with decrease in pressure. However, the Mach number is not design value yet. This can be

a) 0% cowl length

b) 25% cowl length

c) 50% cowl length

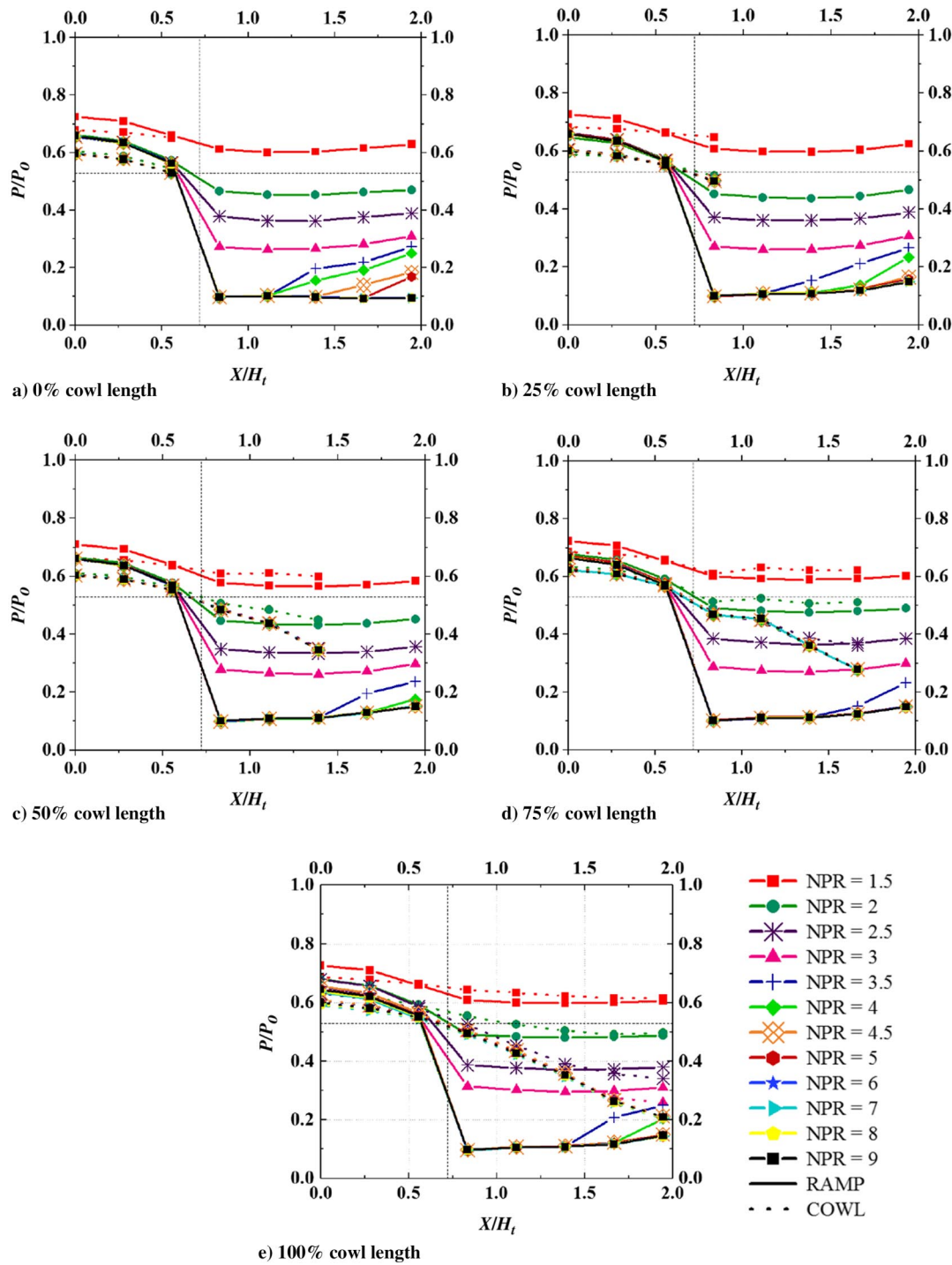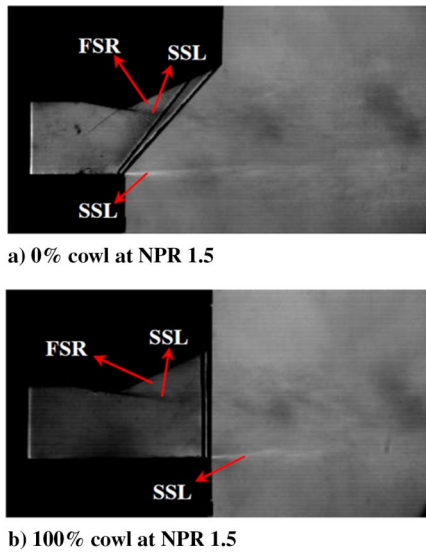d) 75% cowl length

e) 100% cowl length

Fig. 3   Wall static pressure distributions for various cowl lengths at different NPR conditions.

seen from the pressure values not being as low as the high NPR data. The pressure data also show that the flow was separated from the ramp wall for the range of NPRs up to 3. This suggests that the flowfield is similar for all nozzle pressure ratios up to 3. However, there was a gradual increase in the separated shear layer slope as the NPR was increased from 1.5 to 3. The shear layer tends outward and toward the ramp wall as stagnation pressure was increased for 0% cowl and 100% cowl. This is because the pressure in the jet is increasing with the nozzle pressure ratio, and thus there needs to be some expansion for the flow to achieve atmospheric pressure in the jet boundary. This was also observed from the Fig. 3 images for an NPR of 3. Figure 5 shows the shock structure for NPR 3. The 0% cowl length case shows a straight normal shock train with a few

shock cells (SCs), one of which is marked in the image. The 25 and 50% cases also displayed a similar shock train pattern to the 0% cowl case. Whereas 75 and 100% cowl lengths show similar flow-fields, the shock structure appears to be a lambda shock pattern, which includes an incident shock, reflected shock (RS), and a Mach stem (MS) as shown in Fig. 5b.

Increasing the NPR to 3.5, the flow attaches to the ramp wall, which was clearly evidenced from wall static pressures. It can be seen that the wall static pressure in the ramp side is now lower than the exit pressure, and it increases along the downstream direction. This is a typical classical shock in divergent section flow. After the throat, the pressure decreases, and at some location, a sudden jump in the wall static pressure occurs due to a shock. The flow downstream was

a) 0% cowl at NPR 1.5

b) 100% cowl at NPR 1.5

Fig. 4 Schlieren flow visualization images for different cowl lengths at NPR 1.5 (SSL is separated shear layer and FSR is flow-separated region).

subsonic with very gradual change in pressure toward ambient conditions. The shock-induced boundary-layer separation at the ramp section, which prevails in all the cowl length cases, could be observed from Figs. 3a–3e, as was also reported in the literature as shock-induced separation (SIS) [21]. However, in the cowl side, the flow gets more acceleration up to the throat as compared to the ramp, whereas after the throat, the flow expands gradually due to spreading out of expansion fan from the throat corner. The higher acceleration of the ramp section causes the overexpansion leading to SIS was also reported [34].

Figure 6 shows schlieren images for 0, 50, and 100% cowl lengths at various NPR conditions. Images corresponding to 25 and 75% cases are not shown, as the trends from 0 to 100% are smooth. As the NPR increases to 4, Figs. 6a–6c show the schlieren images for 0, 50, and 100% cowl lengths. A small lambda shock (LS) appears for 0% cowl length near the boundary-layer separation on the ramp side, and a large Mach disc is seen in Fig. 6a, with a small expansion near the cowl tip. The Mach disc is also tilted upward, mostly due to the expansion at the throat, to attach to the ramp wall. As the NPR increases further, the flow becomes less overexpanded and tends toward weaker and weaker shocks at the ramp tip. On the cowl tip, the cowl length decides to what extent the expansion fan from the

a) 0% cowl at NPR 3

b) 100% cowl at NPR 3

Fig. 5 Schlieren flow visualization images for different cowl lengths at NPR 3 (ASL is atmospheric shear layer, EF is expansion fan, MD is Mach disc, OS is oblique shock, and TP is triple point).
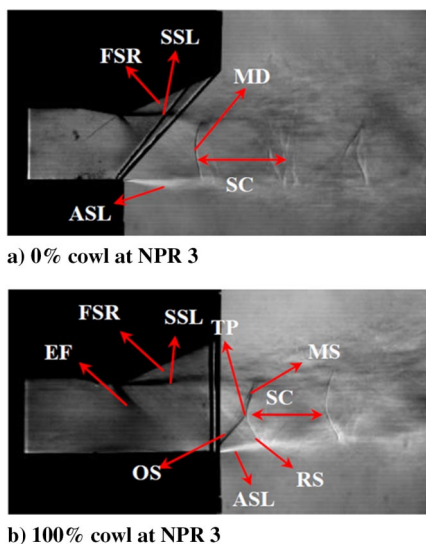
throat corner accelerates the flow before the exit. When there is not much expansion from the throat, the rest of the expansion occurs after the exit and thus forms the underexpanded jet case. The 25, 50, and 75% cowl length cases have a slightly underexpanded feature near the cowl tip, and the Mach disc length decreases as cowl length increases. Similar flow features were observed earlier when the NPR was changed in the SERN [32,35]. The Mach disc appears like a curved shock (CS) in Fig. 6b, which is due to the interaction of the expansion waves from the cowl and the compression waves reflecting from the jet boundary. When the cowl length is higher, the expansion of the flow is complete, and the flow ends up overexpanded at the exit as seen in Fig. 6c. The curved shock now transforms into a Mach disc with oblique shocks from the cowl tip. Thus, the flow features on the cowl tip gradually shift from an underexpanded to overexpanded condition. Similar observations hold true for nozzle pressure ratios 4.5–8, which can be easily noticed by the shear layer slope in the cowl tip in the schlieren images from Figs. 6d–6i.

One can notice that the exit shear layers are almost along the wall slopes for NPR 8 and 100% cowl. This is because NPR 8 approximately corresponds to the perfectly expanded case for this nozzle. NPR 9 becomes the fully underexpanded case for both ramp and cowl tips, as expected from the third critical pressure for the nozzle. Considering the effect of increasing the NPR for a fixed cowl length, it can be seen that as the NPR increases, the flow expands out more in the cowl tip side. This can be seen through the slope of the shear layer at the cowl tip. On the ramp side, as discussed earlier, the flow separates from the throat corner and flows straight in the low NPR of 1.5, and then it expands gradually until the flow is attached to the ramp at above NPR 3. After this, it can be seen that the flow is expanding along the ramp wall and ending up as overexpanded flow, thus forming a shock wave to match the ambient pressure. As the NPR increases, the shock is pushed more downstream as it becomes oblique shock and eventually a weak Mach wave at NPR 8.
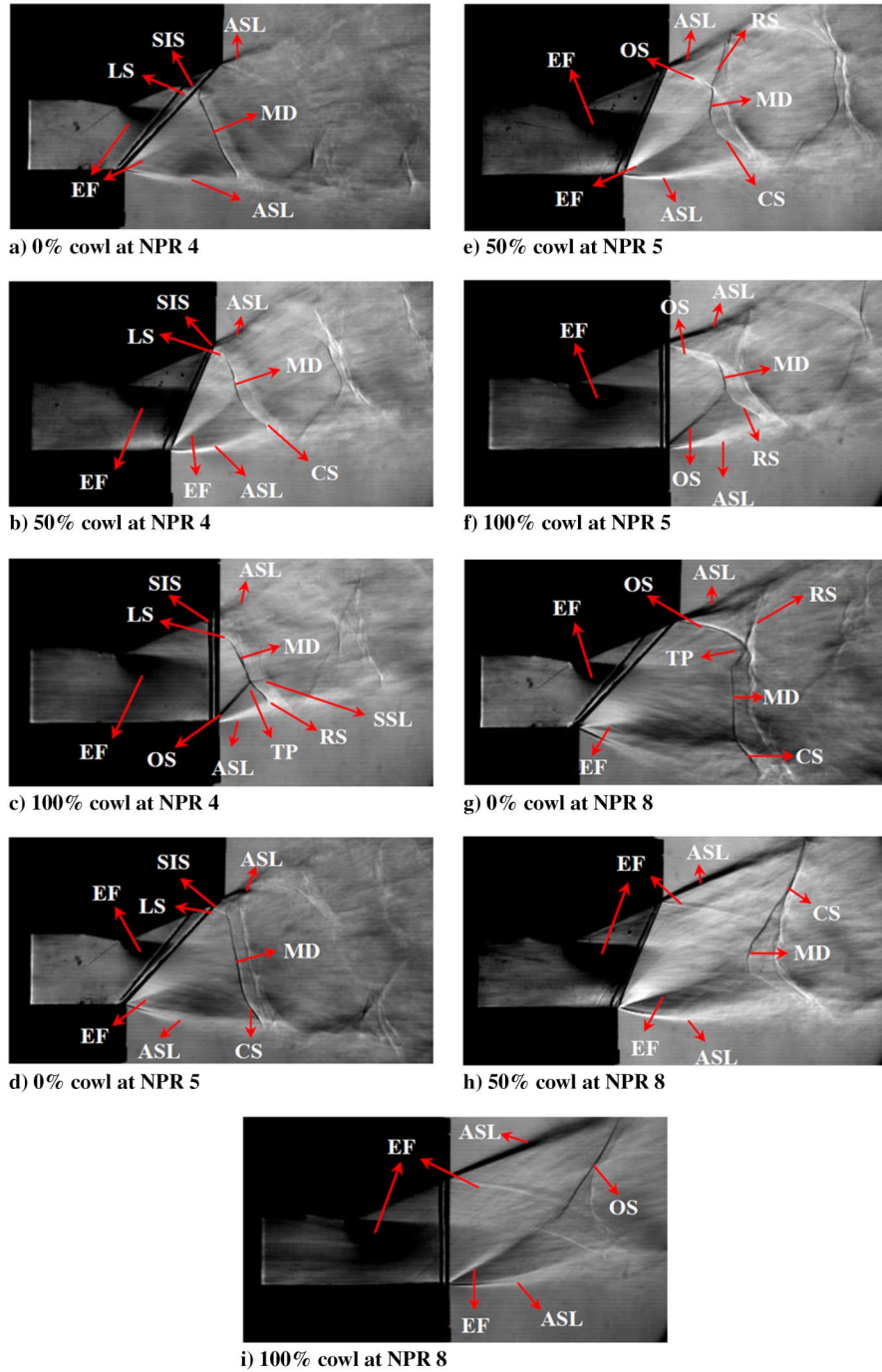
In the jet, the shock from the ramp wall/tip and the expansion from the cowl tip interact to form a partial Mach disc. It is also brought to the notice of the readers here that the edge of the side glass walls will also produce appropriate waves depending on the pressure at the exit, and this will be close to the expansion fan near the cowl and close to a shock near the ramp. All these waves will interact three dimensionally in the downstream. Thus, it is complex to explain the wave pattern present in the jet. However, it can be seen that as a general trend for all attached cases (nozzle pressure ratios 4–9), the shock system appears to be a Mach disc for 0% cowl and becomes more of an X-like shock interaction as cowl length increases. Some of the shocks seen may be due to the interaction of waves from the side wall edge, and one cannot easily recognize this kind of trend in this flowfield, unless through a simulation.

B. Axial, Normal, and Gross Thrust Ratio

The previous subsection attempted to explain the flow features and pressure distributions observed. This subsection provides the internal flow-based performance assessment of the SERN at different NPR conditions, similar to those reported by Deere and Asbury [35] and Capone [36], viz., and various forms of thrust force, such as axial, normal, and gross thrust, in nondimensional form. The performance parameters were estimated from centerline wall static pressure distributions. This method assumes that the wall pressure distribution is the same as that in the centerline. This is usually not true, as the corner flow will have typically higher pressures than the centerline flow. Hence, the estimated axial, normal, and gross thrust ratios will be lesser than the three-dimensional estimates by around 2%, as reported in literature [24,25]. While this estimate could be an underestimate as compared with the results of pressure-sensitive paint-based methods and wind-tunnel testing, this method quickly captures the essential trends in forces with low-cost experiments, and schlieren photographs of the flowfield capture the separation zones and shock patterns. The forces are calculated by considering the surface force integration approach as represented in Fig. 7. The ideal thrust was also estimated from the mass flow rate and ideal velocity, which is calculated from the isentropic relations. The equations used to

a) 0% cowl at NPR 4

e) 50% cowl at NPR 5

b) 50% cowl at NPR 4

f) 100% cowl at NPR 5

c) 100% cowl at NPR 4

g) 0% cowl at NPR 8

d) 0% cowl at NPR 5

h) 50% cowl at NPR 8

i) 100% cowl at NPR 8

Fig. 6   Schlieren flow visualization images for different cowl lengths at NPRs 4, 5, and 8.

estimate the forces, moments, and thrust vectoring angle from the wall static pressure data are mentioned in the following.

Equations (1–3) are used to calculate the axial force and normal force contributed by wall static pressure at the ith port. The inlet section of the SERN also contributes to the axial force, which is estimated from Eq. (4). Hence, the total axial and normal force acting on the entire surface of the SERN is calculated from Eqs. (5) and (6). The gross thrust acting on the SERN is estimated from Eq. (7). The forces were nondimensionalized with respect to an ideal thrust produced by the SERN based on the assumption of isentropic expansion inside the nozzle using Eqs. (8) and (9) [37]. Finally, the thrust vectoring angle and the pitching moment coefficient were estimated from the Eqs. (10) and (11). The procedure for the estimations of uncertainties in the experimental data explained by Rathakrishnan and Kathiravan et al. [38,39] is used. The uncertainties in the measurements of axial force, normal force, gross thrust, thrust vectoring

angle, and pitching moments are estimated as 2.46, 2.39, 3.43, 2.66, and 4.9%, respectively.

$$dF_{X,i} = (P - P_a)\Delta l_i W \sin\beta_i \tag{1}$$

$$dF_{Y,i} = (P - P_a)\Delta l_i W \cos\beta_i \tag{2}$$

$$\Delta l_i = \sqrt{\Delta X_i^2 + \Delta Y_i^2} \tag{3}$$

$$F_f = \oint (P_o - P_a)\, \mathrm{d}A \tag{4}$$

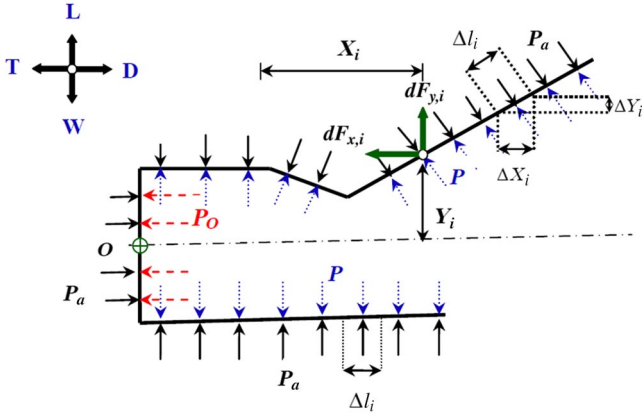$$F_X = F_f + \Sigma dF_{X,i} \tag{5}$$

Fig. 7 Surface force integration approach for force calculation (L = Lift, W = Weight, T = Thrust, and D = Drag).

$$F_Y = \Sigma dF_{Y,i} \tag{6}$$

$$F_g = \sqrt{F_X^2 + F_Y^2} \tag{7}$$

$$F_i = m_a \sqrt{\frac{2\gamma}{\gamma - 1} RT_O \left[1 - \left(\frac{P_a}{P_o}\right)^{(\gamma-1)/\gamma}\right]} \tag{8}$$

$$m_a = \frac{0.6847}{\sqrt{RT_O}} P_o A_t = \rho_t A_t V_t \tag{9}$$

$$\theta = \tan^{-1}\left(\frac{F_Y}{F_X}\right) \tag{10}$$

$$C_m = \frac{\Sigma(dF_{X,i} \times Y_i) + \Sigma(dF_{Y,i} \times X_i)}{P_O A_t H_t} \tag{11}$$

For the estimation of forces and moment from the preceding equations, the assumed values for the parameters were total temperature $T_o = 300$ K, gas constant $R = 287$ kJ/(kg · K), and specific heat ratio $\gamma = 1.4$. The value of Δl_i was the center distance measured across the pressure ports for the force calculation, and it varies with the location of the pressure port. The β_i value at the convergent and divergent section of the concave ramp is 10.3 and 25 deg, respectively. The β_i value used for calculating the value of $F_{x,i}$ for the convergent side had a negative sign and for the divergent side had a positive sign.

Figure 8 shows the variations in nondimensionalized axial thrust for different cowl lengths at NPRs ranging from 1.5 to 9. It can be seen that all the cases of cowl lengths have almost the same trend as the NPR increases: The thrust increases, and then it jumps to a lower value at NPR 3.5 and then again increases continuously until NPR 9. A similar axial thrust variation was also observed in an earlier work [9]. This is because, when the jet is separated from the ramp, as the NPR increases, the pressure in the settling chamber increases, and thus the net thrust increases with pressure, as the ramp wall does not contribute to thrust. When the NPR is 3.5 or more, the jet attaches to the ramp. When the jet is attached to the ramp, the wall pressure on the ramp also contributes to the axial forces. This force is negative as the nozzle is overexpanded, causing the thrust values to drop to lower values when the jet is attached. When the NPR is increased further, the nozzle gets closer to the perfectly expanded condition, and thus the thrust increases.

Upon deeper scrutiny, one can see that the trend of the 0% cowl length case is different from the rest of the cases above NPR 5. This is because the expansion from the cowl lip in this case expands the flow much faster to higher Mach numbers and the ramp-side flow is overexpanded, even at NPR 8, contributing to more drag and reduc-
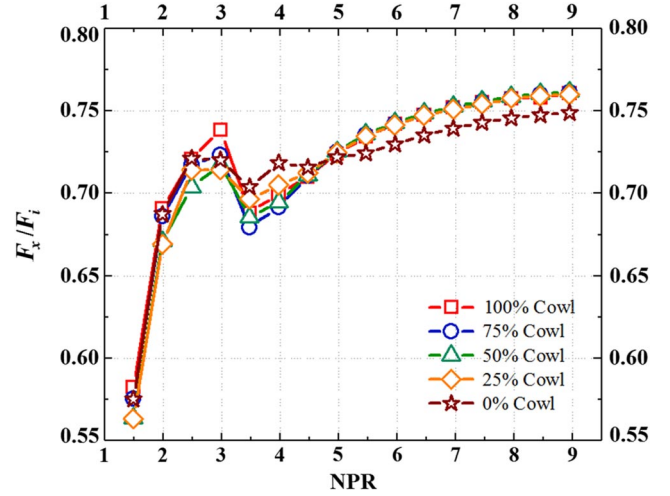

Fig. 8 Axial thrust ratio for different cowl lengths at various NPR conditions.

ing the thrust. This explains the lower thrust for the 0% case above NPR 5 compared to other cases. For NPRs 3.5–5, the 0% case has shock in the ramp with pressures higher than the other cases in the ramp side, causing higher contribution to the thrust, resulting in higher thrust for the 0% case. The 25% case has a similar trend, with slightly weaker shock giving a slightly lesser contribution to the thrust. All the other cowl length cases have almost the same contributions, as the flow has shock outside the nozzle for these cases. For NPRs 1.5–3, there is no attached flow on the ramp, and thus there should ideally not be any effect due to cowl length variation. However, there is a small change in pressure and the wave patterns (as seen from schlieren images), and this may be due to the effect of ramp-side throat expansion waves reflecting off of the cowl for longer cowl cases. The general increase in the thrust force is due to the converging part of the nozzle, which has decreasing pressure as the flow accelerates toward the throat. This produces unbalanced forces in the chamber upstream of the throat (refer to Fig. 7), giving the net positive thrust. This is proportional to the stagnation pressure and thus will increase as the NPR increases. The increase is higher before the nozzle chokes and lowers after choking.

Figure 9 shows the normal force ratio for various cowl length configurations of the SERN. The negative sign represents the normal force acting in a downward direction (toward the cowl), which could induce a nose-up moment for the hypersonic vehicle. The general trend for all the cases is that as the NPR increases, the normal force (which is usually negative) is almost constant (but slightly increasing) up to NPR 2.5, there is a negative jump at NPR 3.5, and after that, the force becomes more negative up to NPR 4 and then it trends upward up to NPR 9. The jump at NPR 3.5 is due to the flow getting attached to the ramp wall. This causes the pressure on the wall to decrease significantly, causing a downward force due to suction. Above NPR 4, the nozzle is generally overexpanded and tending toward the perfectly expanded condition, which causes the suction force on the ramp to decrease; thus, the normal force increases (more force upward) for all the cases from NPR 4 to 9.

As seen in Fig. 9, the 0% cowl case has expansions from the cowl tip overexpanding the ramp wall flow and causes a very strong shock wave at the ramp wall, which causes a good amount of upward force. This explains the trend of force vector tending to point upward, from the 100 to 0% case. The location of the shock in the diverging section at nozzle pressure ratios 3.5 and 4 for various cowl lengths decides the downward force magnitude. Schlieren images show that the shock in the divergent section moves downstream as the cowl length increases. This will result in positive force on the ramp decreasing with increasing length of the cowl. However, a countereffect is that the shock can cause separation, and the separated flow exerts close to ambient pressure on the ramp and thus does not cause much normal force. The flow in the cowl side for NPRs 3–4 is having higher pressures than ambient for up to 75% cowl length, and it becomes less than
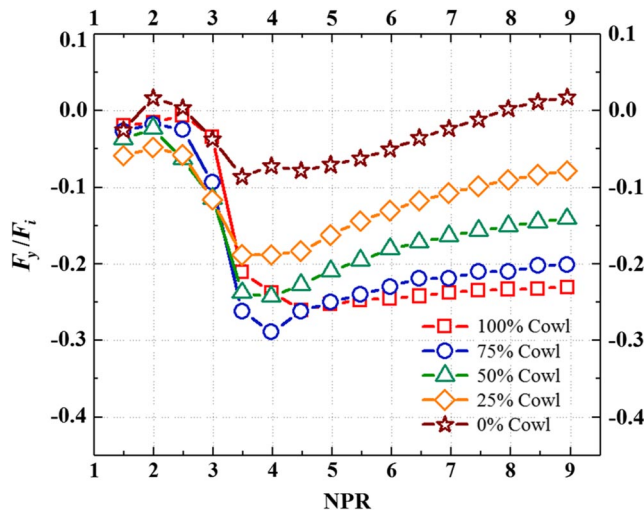
Fig. 9 Normal force ratio for different cowl lengths at various NPR conditions.

Fig. 10 Gross thrust ratio for different cowl lengths at various NPR conditions.

ambient for 100% cowl. This is also shown by the shock/expansion at the cowl trailing edge in the schlieren images shown earlier. This suggests that the cowl with length up to 75% contributes to negative normal force, which is not as severe for the 100% case. This delicate competition between ramp and cowl pressures decides the net normal force for the nozzles. This is the reason for the nonmonotonic trend in the range of NPRs 3–5.

The nozzle pressure ratio 1.5–3 conditions generally have increasing upward force. This can be explained only from the pressure distribution given in Fig. 3. These nozzle pressure ratios have flow detached from the ramp wall for all cowl cases. Thus, the ramp pressure is almost ambient pressure, the cowl pressure is above the ramp pressure in the diverging section, and in the converging section, the cowl pressure is always lower than the ramp wall pressure. Thus, the diverging section produces a downward force, while the converging section produces an upward force. The pressure data show that the difference in pressure is higher in the divergent section, and thus the force is overall negative. As the NPR increases from 1.5 to 3, the flow Mach number increases in the converging section, and thus the pressure ratio decreases. This causes the normalized normal force to decrease in the converging section. This causes a slow increase in this range of nozzle pressure ratios. Since the cowl length is cut off for the different cases, as the cowl length decreases from 100%, it is expected that the downward force decreases. This explanation works well for the 25 to 100% case. The 0% case alone has a peculiar force behavior, which is most likely due to the sonic point shifting upstream due to the extreme pressure gradient in the cowl tip. Thus, the sonic point in the cowl side is more upstream than that in the ramp side, causing higher suction on the cowl wall, contributing to more upward force.

Figure 10 presents the gross thrust as estimated from Eq. (7) and nondimensionalized with ideal thrust conditions. It is basically the normalized magnitude of the vector force on the nozzle, due to both horizontal and vertical forces. Since the individual horizontal and vertical components have been explained in the previous paragraphs, this discussion will only use the values of the components to explain the vector magnitude variations. Equation (7) will always give higher values than the individual components, and the direction of the vertical component is nullified in the expression. Thus, the trends of both Figs. 8 and 9 will be merged in this plot. The major trend in the gross thrust is similar to that observed in Fig. 10, as the thrust component is higher than the vertical component. The 0% case has almost the same trend as thrust force, since the vertical force magnitude is very small and does not contribute significantly to the gross thrust. However, as seen in Fig. 10, all the cases 25 to 100% have the same trend, and from Fig. 10, the vertical force magnitude increases with cowl length. Thus, the gross thrust increases with an increase in
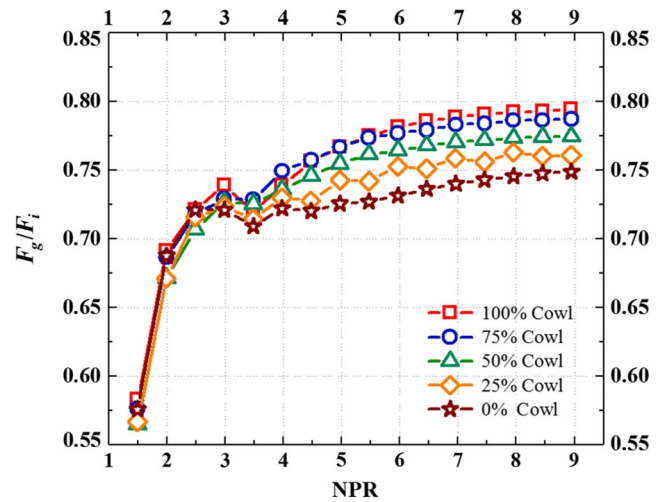
cowl length. The trend of gross thrust increasing with the NPR was also observed by Hirschen et al. [24].

C. Thrust Vectoring Angle and Coefficient of Pitching Moment

The thrust vectoring angle is calculated using the Eq. (10) and presented in Fig. 11. This is basically the vector angle of the gross thrust vector with respect to the incoming flow direction (horizontal). This is mostly negative since the vertical force is mostly negative, as seen in Fig. 11. Equation (10) will be very sensitive to F_Y/F_i trends (for $F_Y < F_X$), and thus Fig. 11 closely follows the trends followed in Fig. 9. The only change in the trend is near NPR 3–4 where there are shocks in the diverging section that alter the trends of F_X and F_Y differently, as explained earlier. The pitching moment coefficient is estimated using Eq. (11) by including the contribution of both F_X and F_Y for calculating the moment about point o, as shown in Fig. 7. As seen from Fig. 7 and Eq. (11), the contribution of F_Y is relatively significant due to the larger X_i moment arm compared to the Y_i moment arm for F_X. The nondimensionalized pitching moment is plotted with respect to the NPR, as shown in Fig. 12. This plot is dominated by the trends in Fig. 12 and is almost identical to those of Fig. 9.

D. Jet Width

Principally, jet width or jet half-width of any nozzle is used to examine the spreading rate or momentum flux distribution of the jet flow. In the present study, the jet axis is very difficult to trace
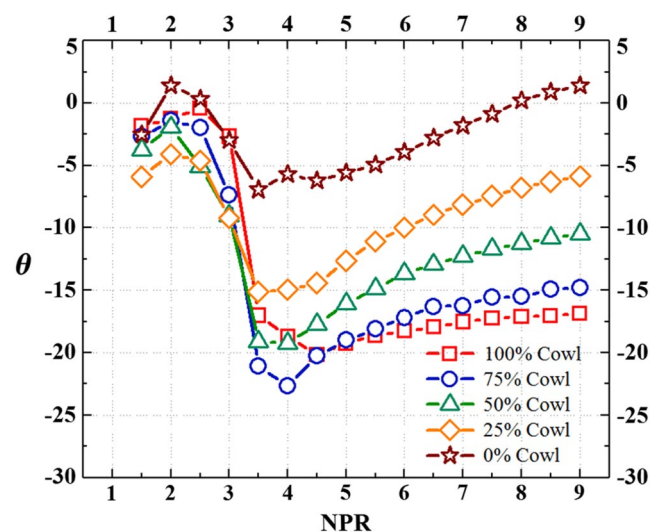

Fig. 11 Pitch thrust vectoring angle for different cowl lengths at various NPR conditions.
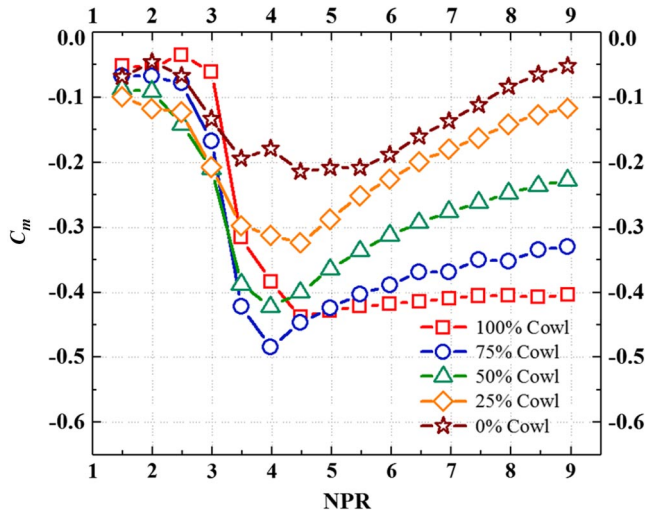
Fig. 12 Coefficient of pitching moment for different cowl lengths at various NPR conditions.

(due to jet deflection) without pitot rake measurements in the jet. Hence, the overall distance between the two shear layers is considered as jet width. Jet widths for different cowl lengths are measured by manually processing the schlieren flow visualization images as shown in Fig. 13. The throat height of the nozzle is considered as the reference length to estimate the jet width. A physical distance of 1 mm is equivalent to 3.3 pixels in the raw image. The uncertainty in the measurement of jet width is 1 pixel, which is approximated to 0.30 mm. The jet width is measured at two locations downstream of the SERN exit, at $X_j/H_t = 1$ and 2 from the ramp tip, for all the cowl length cases.

Figures 14a and 14b show the variation of jet width for several NPR conditions of the SERN at 1 H_t and 2 H_t from the ramp tip. It is evident that the jet width increases along with an increase in the NPR, irrespective of the cowl length variations. The expansion of the jet width in the lateral direction is higher up to NPR 4, and after NPR 5, the rate of spreading decreases. This is because below NPR 4, the jet is expanded in both upward and downward directions by two expansion fans, and after the jet attaches to the ramp wall, the jet shear layer is along the ramp wall and only the cowl side experiences the expansion due to NPR changes, mainly. Since the jet width measurement location is fixed and the shock cells are expanding in the streamwise direction, there is a situation in which the jet waist (at the Mach disc) crosses the measurement location and causes a decrease in the width. This can be seen in a few of the plots, but otherwise the jet widths are increasing with increasing NPRs for both locations.

The variations in the jet width between different cowl lengths at NPR 2 are marginal. Once the NPR increases beyond 3, there is a considerable difference between the successive cowl lengths. Jet width decreases with increasing cowl length. At higher NPR conditions, an approximately 30% difference in jet width is noticed in between 0 and 100% cowl. Similar results are also observed at 2 H_t locations. This is because an increase in cowl length restricts the flow
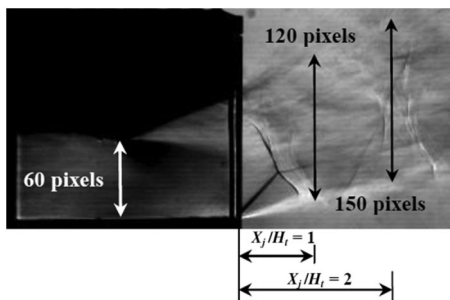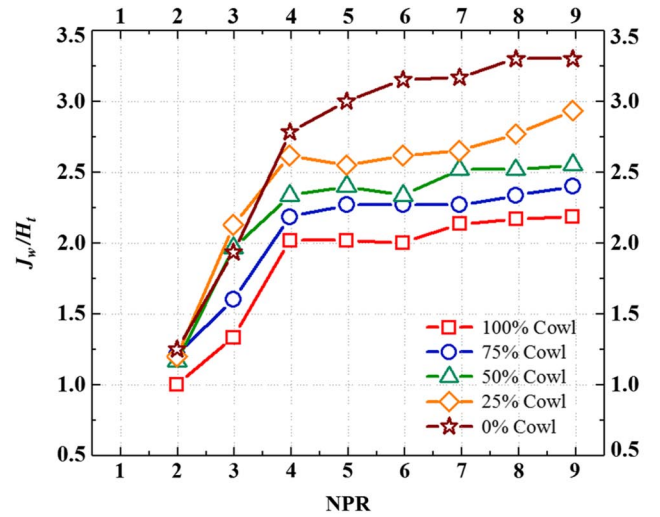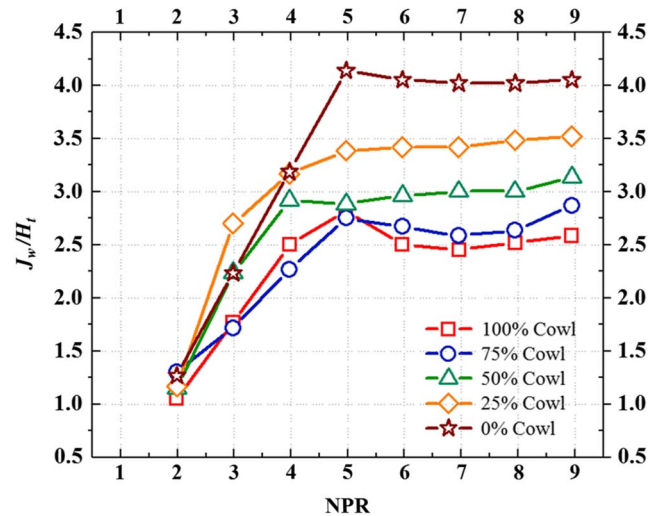

Fig. 13 Simple illustration for jet width calculation.

a) Jet width at 'Ht' location from exit of the ramp section

b) Jet width at '2 Ht' location from exit of the ramp section

Fig. 14 Jet widths for different cowl lengths at various NPR conditions.

expanding in the downward direction progressively, and the jet feature at cowl tip becomes less underexpanded. Thus, the jet width has a tendency to decrease as cowl becomes longer.

IV. Conclusions

Experimental investigations have been performed in an open jet facility to understand the internal flow-based performance and flow characteristic of a concave-type SERN from the wall static pressure measurements. Experiments were conducted at various NPR conditions ranging from 1.5 to 9 for five different cowl lengths, at the design Mach number of 2 corresponding to 100% cowl extension. The following are the major outcomes from this study. At low NPR conditions up to 3, the flow is completely separated from the ramp wall. The jet is along the cowl wall and has shock trains. Longer cowls have lambda shock trains, while shorter cowls have only normal shock trains. The flow gets attached to the ramp wall above NPR 3. The overexpanded condition causes shock-induced separation on the ramp wall. The flow separation moves out as the NPR increases. This movement is delayed in shorter cowls as compared with longer cowls due to lateral expansion near the cowl tip. The cowl side has mostly underexpanded flow, but becomes less underexpanded as cowl length increases. At NPR 8, the flow is perfectly expanded for the 100% cowl case, as it is closest to design. At design condition, the shorter cowl experiences shock waves and Mach disc at the downstream of the nozzle exit, and this might induce loss in performance.

Axial thrust ratio is enhanced by increasing the NPR and is also higher for longer cowls due to more restriction in the lateral direction. A small dip in axial thrust is observed for all geometries when the jet attached to the ramp wall. This dip increases with an increase in cowl length. This sudden variation in the axial thrust ratio might possibly cause vibrations during transient operation of the vehicle. Normal force ratio depends primarily on the flow near the ramp and the cowl walls. Near NPR 3.5, when the flow attached to the ramp wall, the suction increases the negative normal force. As the NPR increases further, the increase in ramp wall pressures causes a general decrease in normal force. As cowl length increases, the normal force becomes more negative, as there is more wall area for pressure to act on. Thus, decreasing the cowl length decreases the pitching moment and the negative lift. The gross thrust ratio increases with increasing nozzle pressure ratio, as expected. The increasing cowl length increases the gross thrust through restricted lateral expansion. Approximately 3–5% less thrust is observed for 0% cowl compared to 100% cowl length, with higher differences for higher nozzle pressure ratios.

The coefficient of pitching moment and thrust vectoring angle are dominated by normal force and follow the same trends. For low nozzle pressure ratios, these parameters depend on the shock pattern on the wall. At higher nozzle pressure ratios, longer cowls will experience higher thrust vectoring and a higher pitching moment. Jet width continuously increases toward high NPR conditions as expected, and the maximum width for a given NPR occurs for a shorter cowl, due to lateral expansion in the cowl side.

Overall, as the NPR increases, axial force and jet width increase, whereas the normal force and the pitching moment increase up to a certain level and then decrease. As the cowl length increases, the axial thrust, normal thrust, pitching moment, and thrust vector angle increase, while the jet width decreases. If one decides to have a high pitching moment or high thrust vectoring, the cowl should be in the range 50–100%, depending on the mission requirement. There is some control actuation possible in terms of NPR variations as well. One can also think of a variable cowl nozzle for this purpose, but this will come with associated cost and weight penalties. It is expected that the trends will be similar even if the design Mach number is higher, as the flow is attached and the performance is dependent on the local wall pressures. The contribution of viscous forces to the drag on the nozzle has not been accounted for in this work.

Acknowledgment

References

[1] Curran, E. T., "Scramjet Engines: The First Forty Years," *Journal of Propulsion and Power*, Vol. 17, No. 6, 2001, pp. 1138–1148.
https://doi.org/10.2514/2.5875

[2] Laitón, S. N. P., de Araujo Martos, J. F., da Silveira Rego, I., Marinho, G. S., and de Paula Toro, P. G., "Experimental Study of Single Expansion Ramp Nozzle Performance Using Pitot Pressure and Static Pressure Measurements," *International Journal of Aerospace Engineering*, Vol. 2019, Feb. 2019, pp. 1–11.
https://doi.org/10.1155/2019/7478129

[3] Kuchar, A. P., and Wolff, J. P., "Preliminary Assessment of Exhaust Systems for High-Mach (4–6) Fighter Aircraft," *Journal of Propulsion and Power*, Vol. 9, No. 4, 1993, pp. 636–643.
https://doi.org/10.2514/3.23668

[4] Otter, J. J., Christiea, R., Goulosa, I., MacManusa, G. D., and Grechb, N., "Parametric Design of Non-Axisymmetric Separate-Jet Aero-Engine Exhaust Systems," *Aerospace Science and Technology*, Vol. 93, Oct. 2019, Paper 105186.
https://doi.org/10.1016/j.ast.2019.05.038

[5] Ruscher, C. J., Magstadt, A. S., Berry, M. G., Glauser, M. N., Shea, P. R., Viswanath, K., Corrigan, A., Gogineni, S., Kiel, B. V., and Giese, A. J., "Investigation of a Supersonic Jet from a Three-Stream Engine Nozzle," *AIAA Journal*, Vol. 56, No. 4, 2018, pp. 1554–1568.
https://doi.org/10.2514/1.J055910

[6] Re, R. J., and Berrier, B. L., "Static Internal Performance of Single Expansion-Ramp Nozzles with Thrust Vectoring and Reversing," NASA TP 1962, March 1982.

[7] Kumar, P. A., and Rathakrishnan, E., "Truncated Triangular Tabs for Supersonic-Jet Control," *Journal of Propulsion and Power*, Vol. 29, No. 1, 2013, pp. 50–65.
https://doi.org/10.2514/1.B34642

[8] Deere, K. A., and Asbury, S. C., "Experimental and Computational Investigation of a Translating Throat Single Expansion-Ramp Nozzle," NASA TP-1999-209138, May 1999.

[9] Capone, F. J., Re, R. J., Bare, E. A., and McLean, M. K., "Parametric Study of Single Expansion Ramp Nozzles at Subsonic/Transonic Speeds," AIAA Paper 1987-1836, July 1987.
https://doi.org/10.2514/6.1987-1836

[10] Damira, S. K., Marathe, A. G., Sudhakar, K., and Issacs, A., "Parametric Optimization of Single Expansion Ramp Nozzle (SERN)," AIAA Paper 2006-5188, July 2006.
https://doi.org/10.2514/6.2006-5188

[11] Marathe, A. G., and Thiagarajan, V., "Effect of Geometric Parameters on the Performance of Single Expansion Ramp Nozzle," AIAA Paper 2005-4429, July 2005.
https://doi.org/10.2514/6.2005-4429

[12] Thiagarajan, V., Panneerselvam, S., and Rathakrishnan, E., "Numerical Flow Visualization of a Single Expansion Ramp Nozzle with Hypersonic External Flow," *Journal of Visualization*, Vol. 9, No. 1, 2006, pp. 91–99.
https://doi.org/10.1007/BF03181572

[13] Kumar, A., and Rathakrishnan, E., "Experimental Investigation of Single Expansion Ramp Performance," *Proceedings of the Institution of Mechanical Engineers, Part G: Journal of Aerospace Engineering*, Vol. 229, No. 7, 2015, pp. 1330–1335.
https://doi.org/10.1177%2F0954410014550051

[14] Schirmer, A. W., and Capone, F. J., "Parametric Study of a Simultaneous Pitch/Yaw Thrust Vectoring Single Expansion Ramp Nozzle," AIAA Paper 1989-2812, July 1989.
https://doi.org/10.2514/6.1989-2812

[15] Yazhini, V., Priyadharshini, S., Kathiravan, B., and Muruganandam, T. M., "Performance Analysis of Single Expansion Ramp Nozzle Under Over-Expanded Condition," *6th National Symposium on Shock Waves*, Paper 58, IIT Madras, Feb. 2020.

[16] Ruffin, M. S., Venkatapathy, E., Keener, R. E., and Spaid, W. F., "Hypersonic Single Expansion Ramp Nozzle Simulations," *Journal of Spacecraft and Rockets*, Vol. 29, No. 6, 1992, pp. 749–755.
https://doi.org/10.2514/3.25527

[17] Watanabe, S., "Scramjet Nozzle Experiment with Hypersonic External Flow," *Journal of Propulsion and Power*, Vol. 9, No. 4, 1993, pp. 521–528.
https://doi.org/10.2514/3.23654

[18] Xu, J., Sha, J., Shi, Z., and Zhang, K., "PIV Experimental Study and Numerical Simulation of the Over-Expanded SERN Exit Jet," AIAA Paper 2008-0099, Jan. 2008.
https://doi.org/10.2514/6.2008-99

[19] Gruhn, P., Henckels, A., and Sieberger, G., "Improvement of the SERN Nozzle Performance by Aerodynamic Flap Design," *Aerospace Science and Technology*, Vol. 6, No. 6, 2002, pp. 395–405.
https://doi.org/10.1016/S1270-9638(02)01177-X

[20] Hiraiwa, T., Tomioka, S., Ueda, S., Mitani, T., Yamamoto, M., and Matsumoto, M., "Performance Variation of Scramjet Nozzle at Various Nozzle Pressure Ratios," *Journal of Propulsion and Power*, Vol. 11, No. 3, 1995, pp. 403–408.
https://doi.org/10.2514/3.23858

[21] Yu, Y., Xu, J., Yu, K., and Mo, J., "Unsteady Transitions of Separation Patterns in Single Expansion Ramp Nozzle," *Shock Waves*, Vol. 25, No. 6, 2015, pp. 623–633.
https://doi.org/10.1007/s00193-015-0595-y

[22] Yu, Y., Xu, J., Mo, J., and Wang, M., "Numerical Investigation of Separation Pattern and Separation Pattern Transition in Overexpanded Single Expansion Ramp Nozzle," *Aeronautical Journal*, Vol. 118, No. 1202, 2014, pp. 399–424.
https://doi.org/10.1017/S0001924000009192

[23] Lv, Z., Xu, J., and Mo, J., "Numerical Investigation of Improving the Performance of a Single Expansion Ramp Nozzle at Off-Design Conditions by Secondary Injection," *Acta Astronautica*, Vol. 133, April 2017, pp. 233–243.
https://doi.org/10.1016/j.actaastro.2017.01.013

[24] Hirschen, C., Gülhan, A., Beck, W. H., and Henne, U., "Measurement of Flow Properties and Thrust on Scramjet Nozzle Using Pressure-Sensitive Paint," *Journal of Propulsion and Power*, Vol. 25, No. 2, 2009, pp. 267–280.
https://doi.org/10.2514/1.37957

[25] Hirschen, C., Gülhan, A., Beck, W. H., and Henne, U., "Experimental Study of a Scramjet Nozzle Flow Using the Pressure-Sensitive-Paint Method," *Journal of Propulsion and Power*, Vol. 24, No. 4, 2008, pp. 662–672.
https://doi.org/10.2514/1.34626

[26] Hirschen, C., and Gülhan, A., "Influence of Heat Capacity Ratio on Pressure and Nozzle Flow of Scramjets," *Journal of Propulsion and Power*, Vol. 25, No. 2, 2009, pp. 303–311.
https://doi.org/10.2514/1.39380

[27] Hirschen, C., and Gülhan, A., "Infrared Thermography and Pitot Pressure Measurements of a Scramjet Nozzle Flowfield," *Journal of Propulsion and Power*, Vol. 25, No. 5, 2009, pp. 1108–1120.
https://doi.org/10.2514/1.41787

[28] Papamoschou, D., Zill, A., and Johnson, A., "Supersonic Flow Separation in Planar Nozzles," *Shock Waves*, Vol. 19, No. 3, 2009, pp. 171–183.
https://doi.org/10.1007/s00193-008-0160-z

[29] Tsunoda, K., Suzuki, T., and Asai, T., "Improvement of the Performance of a Supersonic Nozzle by Riblets," *Journal of Fluids Engineering*, Vol. 122, No. 3, 2000, pp. 585–591.
https://doi.org/10.1115/1.1286991

[30] Zhang, P., Xu, J., Quan, Z., and Mo, J., "Effects of Nonuniform Mach-Number Entrance on Scramjet Nozzle Flowfield and Performance," *Acta Astronautica*, Vol. 129, Dec. 2016, pp. 201–210.
https://doi.org/10.1016/j.actaastro.2016.09.021

[31] Mo, J., Xu, J., Quan, Z., Yu, K., and Lv, Z., "Design and Cold Flow Test of a Scramjet Nozzle with Nonuniform inflow," *Acta Astronautica*, Vol. 108, March 2015, pp. 92–105.
https://doi.org/10.1016/j.actaastro.2014.12.005

[32] Hindash, I., and Spaid, F., "CFD Validation and Wind Tunnel Test for a NASP Single Expansion Ramp Nozzle in the Transonic Regime," AIAA Paper 1991-0015, Jan. 1991.
https://doi.org/10.2514/6.1991-15

[33] Schindel, L., "Effect of Nonuniform Nozzle Flow on Scramjet Performance," *Journal of Propulsion and Power*, Vol. 15, No. 2, 1999, pp. 363–364.
https://doi.org/10.2514/2.5435

[34] Gamble, E., and Haid, D., "Improving Off-Design Nozzle Performance Using Fluidic Injection," AIAA Paper 2004-1206, Jan. 2004.
https://doi.org/10.2514/6.2004-1206

[35] Deere, K. A., and Asbury, S. C., "An Experimental and Computational Investigation of a Translating Throat Single Expansion-Ramp Nozzle," AIAA Paper 1996-2540, July 1996.
https://doi.org/10.2514/6.1996-2540

[36] Capone, F. J., "Static Performance of Five Twin-Engine Nonaxisymmetric Nozzles with Vectoring and Reversing Capability," NASA TP 1224, July 1978.

[37] Mo, J., Xu, J., Gu, R., and Fan, Z., "Design of an Asymmetric Scramjet Nozzle with Circular to Rectangular Shape Transition," *Journal of Propulsion and Power*, Vol. 30, No. 3, 2014, pp. 812–819.
https://doi.org/10.2514/1.B34949

[38] Rathakrishnan, E., *Instrumentation, Measurements and Experiments in Fluids*, 2nd ed., CRC Press, Boca Raton, FL, 2007, pp. 559–573.

[39] Kathiravan, B., Senthilkumar, C., Rajak, R., and Jayaraman, K., "Acoustic Pressure Oscillation Effects on Mean Burning Rates of Plateau Propellants," *Combustion and Flame*, Vol. 226, April 2021, pp. 69–86.
https://doi.org/10.1016/j.combustflame.2020.11.018

R. D. Bowersox
Associate Editor